Article

Cell Host & Microbe

IL-22 Upregulates Epithelial Claudin-2 to Drive Diarrhea and Enteric Pathogen Clearance

Graphical Abstract

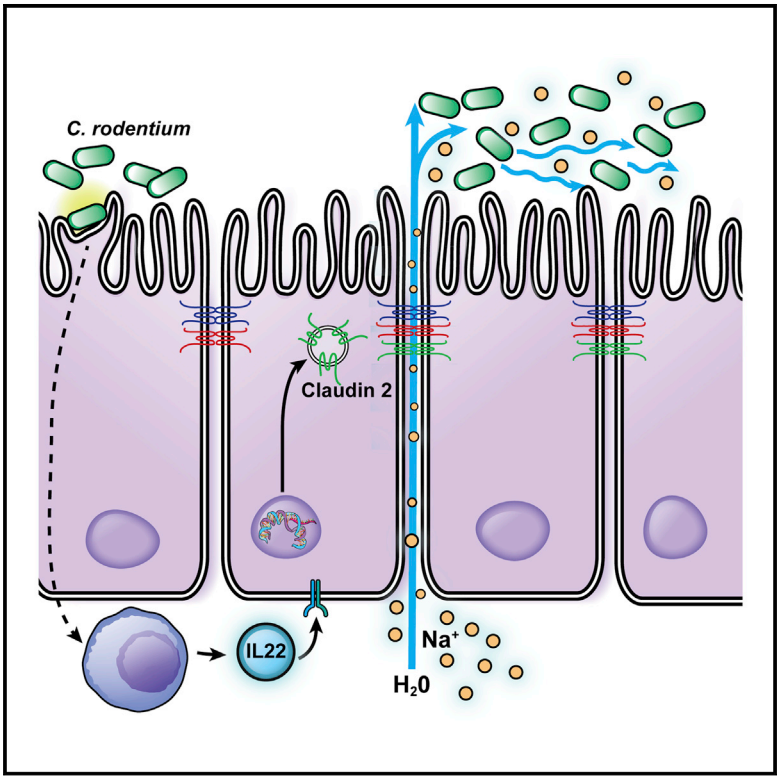

Authors

Pei-Yun Tsai, Bingkun Zhang, Wei-Qi He, ..., Yang-Xin Fu, Sachiko Tsukita, Jerrold R. Turner

Correspondence

jrturner@bwh.harvard.edu

In Brief

Diarrhea is common in enteric infection, but whether this reflects disease progression or host defense is unknown. Using the *C. rodentium* model, Tsai et al. show that diarrhea is critical to pathogen clearance and demonstrate that diarrhea development requires claudin-2 upregulation that increases tight junction permeability to Na^+ and water.

Highlights

- IL-22 induced by enteric infection upregulates the tight junction protein claudin-2
- Intestinal epithelial claudin-2 expression promotes paracellular Na^+ and water efflux
- Na^+ and water efflux results in diarrhea that facilitates pathogen clearance
- Claudin-2-mediated diarrhea is an innate mechanism of host defense

Tsai et al., 2017, Cell Host & Microbe *21*, 671–681
June 14, 2017
http://dx.doi.org/10.1016/j.chom.2017.05.009

Cell Host & Microbe
Article

IL-22 Upregulates Epithelial Claudin-2 to Drive Diarrhea and Enteric Pathogen Clearance

Pei-Yun Tsai,[2,8] Bingkun Zhang,[1,2,8] Wei-Qi He,[2,3] Juan-Min Zha,[2,3,4] Matthew A. Odenwald,[2] Gurminder Singh,[2,6] Atsushi Tamura,[5] Le Shen,[2] Anne Sailer,[2] Sunil Yeruva,[2,6] Wei-Ting Kuo,[6] Yang-Xin Fu,[2,7] Sachiko Tsukita,[5] and Jerrold R. Turner[2,6,9,*]

[1]State Key Laboratory of Animal Nutrition, Department of Animal Nutrition & Feed Science, College of Animal Science & Technology, China Agricultural University, Haidian District, Beijing 100193, China
[2]Department of Pathology, The University of Chicago, 5841 South Maryland, Chicago, IL 60637, USA
[3]Cambridge-Suda (CAM-SU) Genome Resource Center, Soochow University, Suzhou 215123, China
[4]Department of Oncology, The First Affiliated Hospital of Soochow University, Suzhou 215006, China
[5]Laboratory of Biological Science, Graduate School of Frontier Biosciences and Graduate School of Medicine, Osaka University, Osaka, 565-0871, Japan
[6]Departments of Pathology and Medicine (Gastroenterology), Brigham and Women's Hospital and Harvard Medical School, Boston, MA 02115, USA
[7]Department of Pathology, University of Texas Southwestern, Dallas, TX 75235, USA
[8]These authors contributed equally
[9]Lead Contact
*Correspondence: jrturner@bwh.harvard.edu
http://dx.doi.org/10.1016/j.chom.2017.05.009

SUMMARY

Diarrhea is a host response to enteric pathogens, but its impact on pathogenesis remains poorly defined. By infecting mice with the attaching and effacing bacteria *Citrobacter rodentium*, we defined the mechanisms and contributions of diarrhea and intestinal barrier loss to host defense. Increased permeability occurred within 2 days of infection and coincided with IL-22-dependent upregulation of the epithelial tight junction protein claudin-2. Permeability increases were limited to small molecules, as expected for the paracellular water and Na^+ channel formed by claudin-2. Relative to wild-type, claudin-2-deficient mice experienced severe disease, including increased mucosal colonization by *C. rodentium*, prolonged pathogen shedding, exaggerated cytokine responses, and greater tissue injury. Conversely, transgenic claudin-2 overexpression reduced disease severity. Chemically induced osmotic diarrhea reduced colitis severity and *C. rodentium* burden in claudin-2-deficient, but not transgenic, mice, demonstrating that claudin-2-mediated protection is the result of enhanced water efflux. Thus, IL-22-induced claudin-2 upregulation drives diarrhea and pathogen clearance.

INTRODUCTION

The intestinal barrier is often compromised during enteric infection. In the case of invasive and toxigenic organisms, this typically involves direct epithelial damage. In contrast, non-invasive, attaching and effacing (A/E) pathogens, such as the human and mouse pathogens enteropathogenic *E. coli* and *Citrobacter rodentium*, respectively, use a type III secretion system to inject proteins into host cells (Deng et al., 2010). These effector proteins promote cytoskeletal reorganization and increase intestinal permeability (Guttman et al., 2006). However, neither the mechanisms that underlie these permeability increases nor their significance to pathogenesis are well understood.

Intercellular tight junctions define the epithelial paracellular barrier but do not form an absolute seal, as paracellular permeability is necessary for ion, water, nutrient, and waste transport. Flux across tight junctions occurs by two distinct routes, defined as the pore and leak pathways (Figure 1A). The pore pathway is a high-capacity, charge- and size-selective route with a maximum diameter of 6 Å (Anderson and Van Itallie, 2009; Turner, 2009). In contrast, the low conductance leak pathway is relatively nonselective and accommodates molecules with diameters up to ~100 Å. Finally, materials can cross the barrier via the unrestricted pathway (Figure 1A), which allows free passage of ions, water, macromolecules, bacteria, and viruses as a result of epithelial damage. The unrestricted pathway is therefore tight junction independent.

Barrier loss in disease is frequently attributed to tight junction dysregulation, but the tools used in most in vivo analyses cannot discriminate between increased tight junction permeability and epithelial damage. As a result, the relative contributions of the pore, leak, and unrestricted pathways to intestinal barrier loss, disease progression, and host responses during enteric infection have not been defined. We developed an in vivo assay that allowed independent analysis of each permeability pathway (Figure 1A) during *C. rodentium* colitis. This made it possible to identify an early increase in pore pathway permeability resulting from IL-22-dependent claudin-2 upregulation. Genetic and pharmacological interventions showed that this claudin-2-mediated increase in pore pathway permeability increased water efflux and enhanced *C. rodentium* clearance. These results identify an unrecognized mechanism of IL-22-dependent host defense

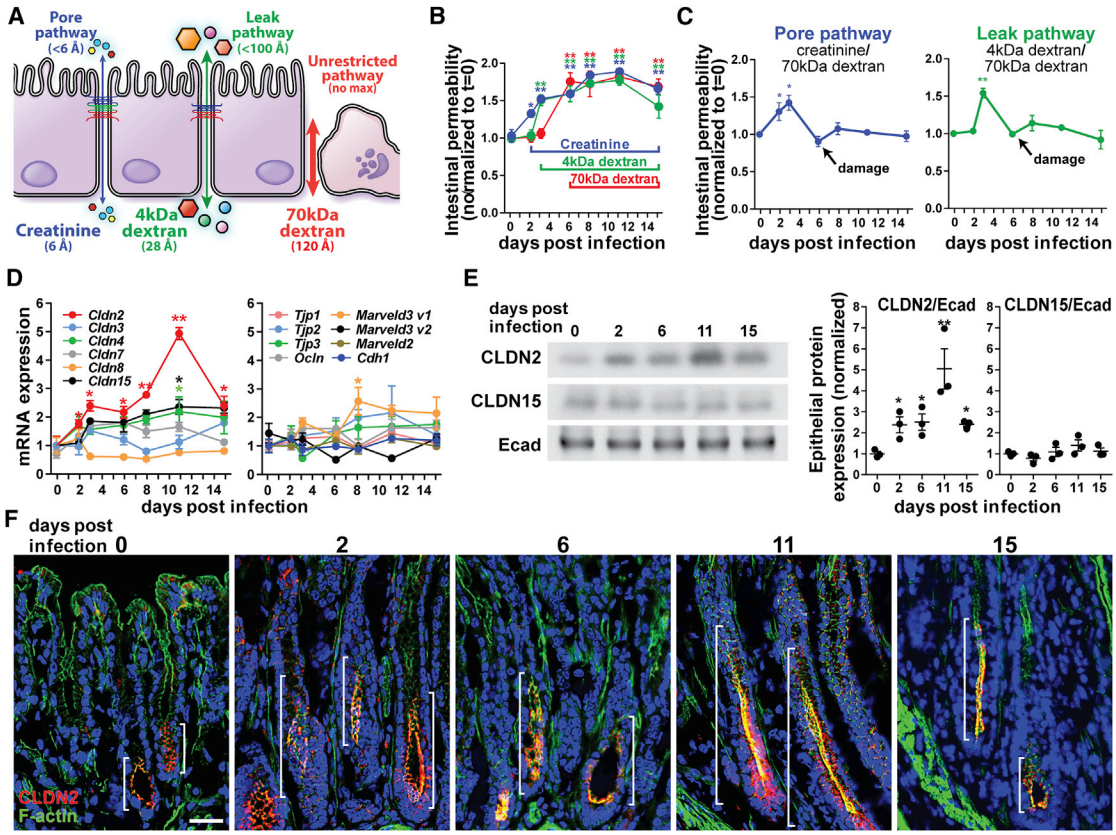

Figure 1. Pore Pathway Permeability and Claudin-2 Expression Are Increased Early in the Course of *C. rodentium* Infection

(A) Pore, leak, and unrestricted pathway permeabilities were assessed using creatinine, 4 kDa dextran, and 70 kDa dextran, respectively.

(B) Creatinine, 4 kDa dextran, and 70 kDa dextran fluxes increased 2, 4, and 6 days after infection, respectively (n = 6). Error bar represents mean ± SEM. *p < 0.05, **p < 0.01.

(C) Specific pore and leak pathway permeabilities increased shortly after *C. rodentium* infection but were undetectable by day 6 due to epithelial damage. Creatinine and 4 kDa dextran flux at these times therefore reflects increased unrestricted pathway, not tight junction, permeability. Error bar represents mean ± SEM. *p < 0.05, **p < 0.01.

(D) Quantitative RT-PCR analysis shows that only claudin-2 mRNA is significantly increased at day 2 of infection. Error bar represents mean ± SEM. *p < 0.05, **p < 0.01.

(E) Western blots and densitometry of isolated colonic epithelial cells demonstrate increased claudin-2 (CLDN2), but not claudin-15 (CLDN15) or E-cadherin (Ecad), expression. Error bar represents mean ± SEM. *p < 0.05, **p < 0.01.

(F) Immunofluorescence microscopy shows claudin-2 (red), F-actin (green), and DNA (blue) during infection. Brackets indicate zone of claudin-2 expression. Scale bar represents 50 μm.

and elucidate the essential roles of tight junction regulation and diarrhea in enteric pathogen clearance.

RESULTS

C. rodentium Infection Disrupts the Intestinal Barrier in Three Distinct Phases

C. rodentium infection disrupts the intestinal barrier, but the evolution of barrier loss and its role in disease pathogenesis have not been determined. Most studies have relied on a single probe, FITC-4 kDa dextran, which cannot distinguish between leak and unrestricted pathways (Figure 1A). We characterized barrier loss during disease progression using three probes: creatinine, FITC-4 kDa dextran, and rhodamine-70 kDa dextran, which have hydrodynamic diameters of 6 Å, 28 Å, and 120 Å, and can be used to probe pore, leak, and unrestricted pathways, respectively (Figure 1A).

Intestinal permeability to creatinine was elevated within 2 days of *C. rodentium* infection and continued to increase thereafter (Figure 1B). 4 kDa dextran permeability increased 1 day later, but 70 kDa dextran flux did not increase until day 6 of infection. To specifically asses pore and leak pathways, creatinine or 4 kDa dextran fluxes were normalized to 70 kDa dextran permeability. These ratiometric analyses demonstrated specific increases in pore and leak pathways at 2 and 3 days post-infection, respectively (Figure 1C). The increased 70 kDa dextran permeability that occurred as a result of epithelial damage and increased unrestricted pathway flux at day 6 caused pore and leak pathway ratios to return to baseline values (Figure 1C). The increased creatinine and 4 kDa dextran flux at 6 days after *C. rodentium* infection and beyond is therefore a function of unrestricted pathway permeability rather than specific upregulation of tight junction pore and leak pathways.

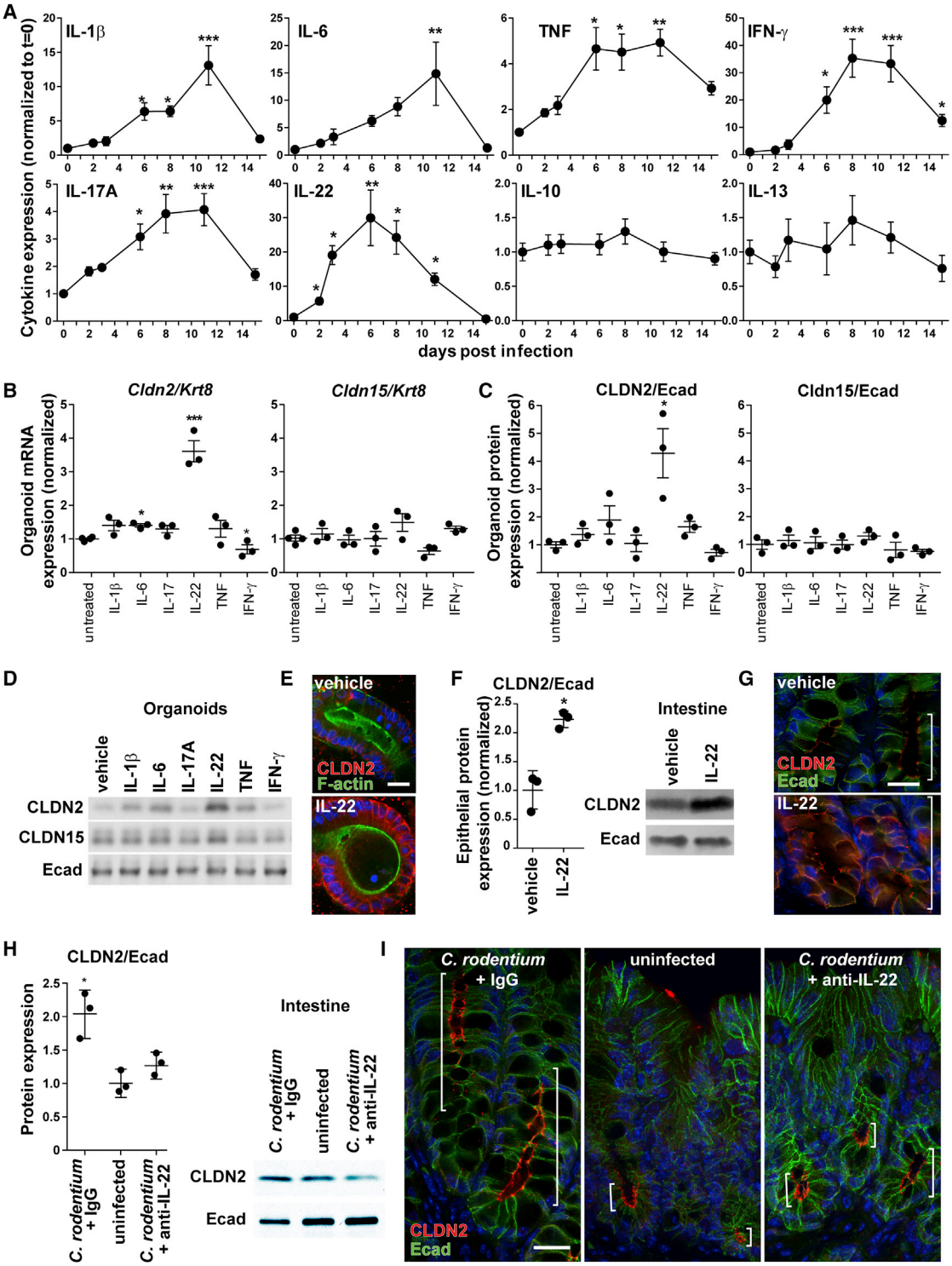

Figure 2. IL-22 Induces Claudin-2 Expression during *C. rodentium* Infection

(A) Cytokine expression at indicated times during *C. rodentium* infection (n = 6). Error bar represents mean ± SEM. *p < 0.05, **p < 0.01, ***p < 0.001.

(B–D) IL-22 upregulates claudin-2 mRNA and protein expression in mouse organoids, as shown by qRT-PCR (B, n=3), western blots (C), and densitometry (D, n = 3). Error bar represents mean ± SEM. *p < 0.05, ***p < 0.001.

(E) Immunofluorescence microscopy of IL-22-treated organoids demonstrates increased claudin-2 (red) expression at tight junctions and lateral membranes. F-actin (green), DNA (blue). Scale bar represents 20 μm.

(F) Western blots and densitometry of claudin-2 (CLDN2) and E-cadherin (Ecad) expression in isolated colonic epithelial cells after in vivo IL-22 treatment (n = 3). Error bar represents mean ± SEM. *p < 0.05.

(legend continued on next page)

Increased Pore Pathway Permeability Is Accompanied by Increased Epithelial Claudin-2 Expression

Pore pathway permeability is primarily regulated by claudin protein expression and function. Quantitative RT-PCR analyses of isolated colonocytes showed that claudin-2 mRNA was uniquely upregulated within 2 days of *C. rodentium* infection (Figure 1D). Limited increases in mRNA encoding *Cldn15*, which complements claudin-2 functionally (Wada et al., 2013), were only significant at day 11. mRNA encoding other tight junction proteins was unchanged in the first week of infection (Figure 1D). Immunoblots confirmed increased claudin-2 protein expression within 2 days of *C. rodentium* infection (Figure 1E).

Immunofluorescence microscopy demonstrated expansion of the zone of claudin-2 expression within 2 days of infection (Figure 1F), well before histologically detectable inflammatory changes or epithelial damage were present (Figure S1). Claudin-2 expression within transit-amplifying cells peaked by day 11 and, consistent with qRT-PCR and western blot data, regressed by day 15 of infection (Figures 1E and 1F). Although marked mucosal hyperplasia does occur during *C. rodentium* infection, the absence of increased claudin-15 expression demonstrates that claudin-2 is specifically upregulated and not merely a consequence of increased cell numbers (Figures 1D and 1E). Given the well-established role of claudin-2 as a mediator of pore pathway permeability, these data suggest that claudin-2 upregulation drives the increased pore pathway permeability detected within 2 days of infection.

C. rodentium Upregulates Claudin-2 via IL-22 Signaling

Cytokine-mediated claudin-2 transcriptional regulation has been described in vitro and in vivo (Mankertz et al., 2009; Suzuki et al., 2011; Weber et al., 2010). Analyses of mucosal cytokines during infection showed that only IL-22 was significantly increased by day 2 (Figure 2A). IL-22 has not, however, been reported to regulate claudin-2 transcription. Cytokines that have been linked to claudin-2 upregulation were increased only at later times (IL-6, TNF, IL-17A) or were unchanged (IL-13).

Despite many advantages, the presence of numerous cell types and potential for complex intercellular signaling limit utility of in vivo models to determine whether IL-22 signals directly to intestinal epithelia. We used intestinal epithelial organoid cultures to overcome this limitation. In organoid cultures IL-22 significantly upregulated claudin-2, but not claudin-15, mRNA and protein expression (Figures 2B–2D). Induced claudin-2 was localized to tight junctions and lateral membranes (Figure 2E). IL-22 is therefore a direct, potent, and selective inducer of epithelial claudin-2.

To determine whether IL-22 could induce claudin-2 upregulation in vivo, wild-type mice were treated with recombinant IL-22. This increased colonic epithelial claudin-2 expression within 24 hr (Figure 2F). Similar to upregulation during infection, both the magnitude of claudin-2 expression within individual cells and the number of cells expressing claudin-2 were increased (Figure 2G). IL-22 is therefore sufficient to induce colonic epithelial claudin-2 expression in vivo. We cannot, however, exclude contributions from other cytokines at later times during *C. rodentium* infection, as IL-22 expression peaks at 6 days after infection, but claudin-2 upregulation progresses until day 11.

The essential contributions of IL-22 to host defense (Zheng et al., 2008) constrain use of IL-22-deficient mice to further probe the role of IL-22 in claudin-2 upregulation during advanced *C. rodentium* infection. However, such comparisons are possible at 2 days after *C. rodentium* infection, when claudin-2 upregulation first occurs, as no differences between wild-type and either IL-22-deficient or anti-IL-22-treated mice are apparent at this early time. Treatment with anti-IL-22 prior to infection prevented *C. rodentium*-induced increases in claudin-2 expression (Figures 2H and 2I). In contrast, robust claudin-2 upregulation was apparent in mice treated with a control IgG (Figures 2H and 2I). These data show that IL-22 is essential for claudin-2 induction during early stages of *C. rodentium* infection. Claudin-2 upregulation may therefore be an unrecognized mechanism by which IL-22 activates innate host defense.

Transgenic Claudin-2 Expression Increases Fecal Na^+ and Water Content

To define the impact of intestinal epithelial claudin-2 expression on *C. rodentium* infection, transgenic mice with intestinal epithelial specific expression of EGFP-claudin-2, which we have shown to be functional (Raleigh et al., 2011), were developed. Analyses of isolated colonic epithelial cells from uninfected claudin-2 transgenic, wild-type, and claudin-2 knockout (Wada et al., 2013) mice showed a 12-fold increase in claudin-2 mRNA in transgenic mice relative to wild-type littermates (Figure 3A). Endogenous claudin-2 protein was expressed at similar levels in wild-type and transgenic mice, but EGFP-claudin-2 expression was 8-fold greater than endogenous claudin-2 (Figure 3B). No claudin-2 transcripts or protein were detected in knockout mice (Figures 3A and 3B). Neither claudin-2 overexpression nor claudin-2 deficiency affected mRNA or protein expression of claudin-15 or any other tight junction components (Figures 3A and 3B).

Neither transgenic claudin-2 expression nor claudin-2 knockout affected colonic histology (Figure 3C). Nevertheless, fluorescence microscopy demonstrated that EGFP-claudin-2 was expressed within an expanded population of epithelial cells (Figure 3D). Thus, both the magnitude and distribution of total claudin-2 expression in uninfected claudin-2 transgenic mice are similar to that in *C. rodentium*-infected wild-type mice. Claudin-2 transgenic mice can, therefore, be used to represent maximal claudin-2 expression. Conversely, claudin-2 knockout mice can be used to model the low endogenous claudin-2 expression seen in adult mice (Holmes et al., 2006; Wada et al., 2013). Claudin-2 transgenic and knockout mice can therefore serve as stable reference points for the low and high claudin-2 expression, respectively, seen in wild-type mice before and during infection.

(G) Claudin-2 (red) expression after IL-22 treatment in vivo. F-actin (green), DNA (blue). Brackets indicate zone of claudin-2 expression. Scale bar represents 20 μm.

(H) Western blots and densitometry of claudin-2 (CLDN2) and E-cadherin (Ecad) expression in isolated colonic epithelial cells from mice pre-treated with control IgG or anti-IL-22 after 2 days of infection (n = 3). Error bar represents mean ± SEM. *$p < 0.05$.

(I) Immunofluorescence microscopy of claudin-2 (red) expression after *C. rodentium* infection in mice pre-treated with control IgG or anti-IL-22 at day 2 of infection. Uninfected mice are shown for reference. E-cadherin (green), DNA (blue). Brackets indicate zone of claudin-2 expression. Scale bar represents 20 μm.

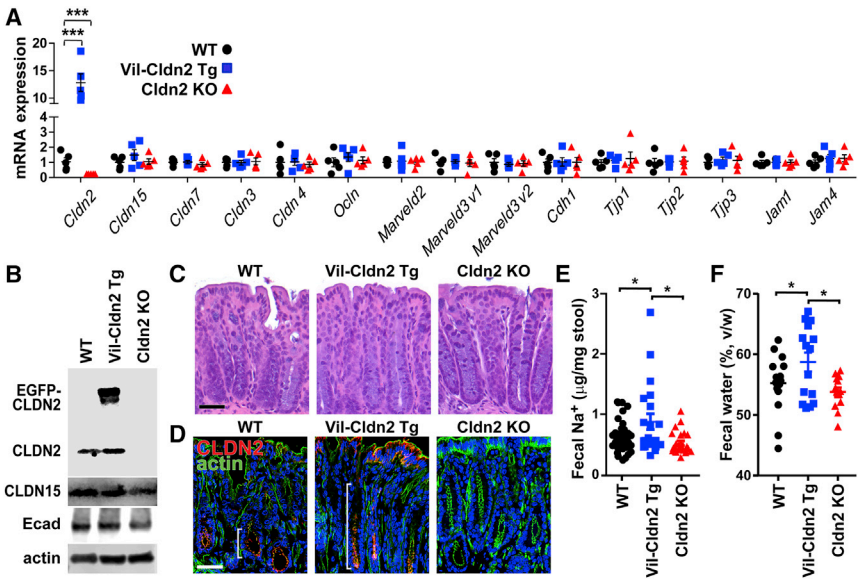

Figure 3. Transgenic Claudin-2 Expression Increases Fecal Na^+ and Water

(A) Tight junction protein mRNA expression in wild-type (WT), claudin-2 transgenic (Vil-Cldn2 Tg), and claudin-2 knockout (Cldn2 KO) mice (n = 5). Only claudin-2 expression differed between genotypes. Error bar represents mean ± SEM. ***p < 0.001.

(B) Immunoblots of claudin-2 (21 kDa) and EGFP-claudin-2 (48 kDa), claudin-15 (21 kDa), E-cadherin (80 kDa), and β-actin (42 kDa).

(C) Histology of wild-type, claudin-2 transgenic, and claudin-2 knockout mice. Scale bar represents 50 μm.

(D) Immunofluorescent microscopy of claudin-2 and EGFP-claudin-2 (red), F-actin (green), and DNA (blue). Brackets indicate zone of claudin-2 expression. Scale bar represents 50 μm.

(E) Fecal Na^+ content of wild-type, claudin-2 transgenic, and claudin-2 knockout mice (n ≥ 21). Error bar represents mean ± SEM. *p < 0.05.

(F) Fecal water content of wild-type, claudin-2 transgenic, and claudin-2 knockout mice (n = 15). Error bar represents mean ± SEM. *p < 0.05.

Uninfected claudin-2 transgenic mice demonstrated significantly increased fecal Na^+ relative to wild-type or claudin-2 knockout mice (Figure 3E), thereby demonstrating that the transgenically expressed EGFP-claudin-2 did function as a cation channel. Further, fecal water, defined as the fraction of total stool mass lost upon desiccation, of claudin-2 transgenic mice was significantly greater than that of wild-type or claudin-2 knockout mice (Figure 3F). These data, which confirm that EGFP-claudin-2 is functional, are consistent with the ability of claudin-2 to conduct Na^+ and water across the tight junction (Rosenthal et al., 2017). As expected given the low claudin-2 expression in adult mice, fecal Na^+ and water content were similar in wild-type and claudin-2 knockout mice (Figure 3F).

Claudin-2 Promotes *C. rodentium* Clearance and Limits Mucosal Immune Activation

C. rodentium infection induced significant weight loss in claudin-2 knockout mice (Figure 4A). In contrast, neither wild-type nor claudin-2 transgenic mice lost weight, as is typical of *C. rodentium* colitis. In addition to weight loss, fecal *C. rodentium* shedding in claudin-2 knockout mice was increased 10-fold on day 9 and 100-fold on days 15 and 18 of infection relative to wild-type or transgenic mice (Figure 4B). On day 11 of infection, which represents both the nadir of body weight in claudin-2 knockout mice (Figure 4A) and the peak of claudin-2 expression in wild-type mice (Figures 1D–1F), wild-type and claudin-2 transgenic mice had 8- and 40-fold fewer mucosa-associated *C. rodentium* than claudin-2 knockout mice, respectively (Figure 4C). These differences in mucosal colonization were evident morphologically, as bacteria penetrated into colonic crypts of claudin-2 knockout mice, yet were restricted to the surface in wild-type and transgenic mice (Figure 4D, arrows). Although this could reflect an effect of claudin-2 on *C. rodentium* colonization, the observation that claudin-2 knockout, claudin-2 transgenic, and wild-type mice shed similar numbers of fecal *C. rodentium* until day 9 suggests that overall colonization was not affected by claudin-2 expression.

Increased mucosal *C. rodentium* numbers might be expected to result in greater immune activation in claudin-2 knockout mice. Consistent with this, infection-associated IL-1β, IL-6, IL-22, and TNF expression were significantly greater in knockout, relative to wild-type or transgenic, mice (Figure 4E). Conversely, TNF expression was significantly reduced in claudin-2 transgenic mice. These differences were not due to pre-existing alterations, as mucosal IL-1β, IL-6, IL-17, IL-22, TNF, and IFN-γ expression were similar in uninfected wild-type, claudin-2 transgenic, and claudin-2 knockout mice (Figure 4E). The markedly increased IL-22 expression in infected claudin-2 knockout mice further suggests that claudin-2 may participate in a negative feedback loop that, by reducing IL-22 production, limits the degree of claudin-2 upregulation.

Claudin-2 Upregulation Limits *C. rodentium*-Induced Tissue Damage

Transgenic expression or knockout of claudin-2 had no effect on intestinal epithelial proliferation or apoptosis in healthy mice (Figure 5A). *C. rodentium* infection markedly increased epithelial proliferation and apoptosis in all mice, but these changes were far greater in claudin-2 knockout, relative to wild-type or transgenic, mice (Figure 5A). The greater epithelial damage and proliferative responses of claudin-2 knockout mice to infection were accompanied by significantly more severe colonic histopathology. While isolated intraepithelial neutrophils were readily identified in wild-type and claudin-2 transgenic mice, neutrophil aggregates were associated with surface epithelial erosions in claudin-2 knockout mice (Figure 5B, arrows).

Consistent with the presence of surface erosions and more frequent apoptotic epithelial cells, increases in creatinine, 4 kDa dextran, and 70 kDa dextran permeability were exaggerated in *C. rodentium*-infected claudin-2 knockout mice at day 11 of infection (Figure 5C). However, the increases for each probe were

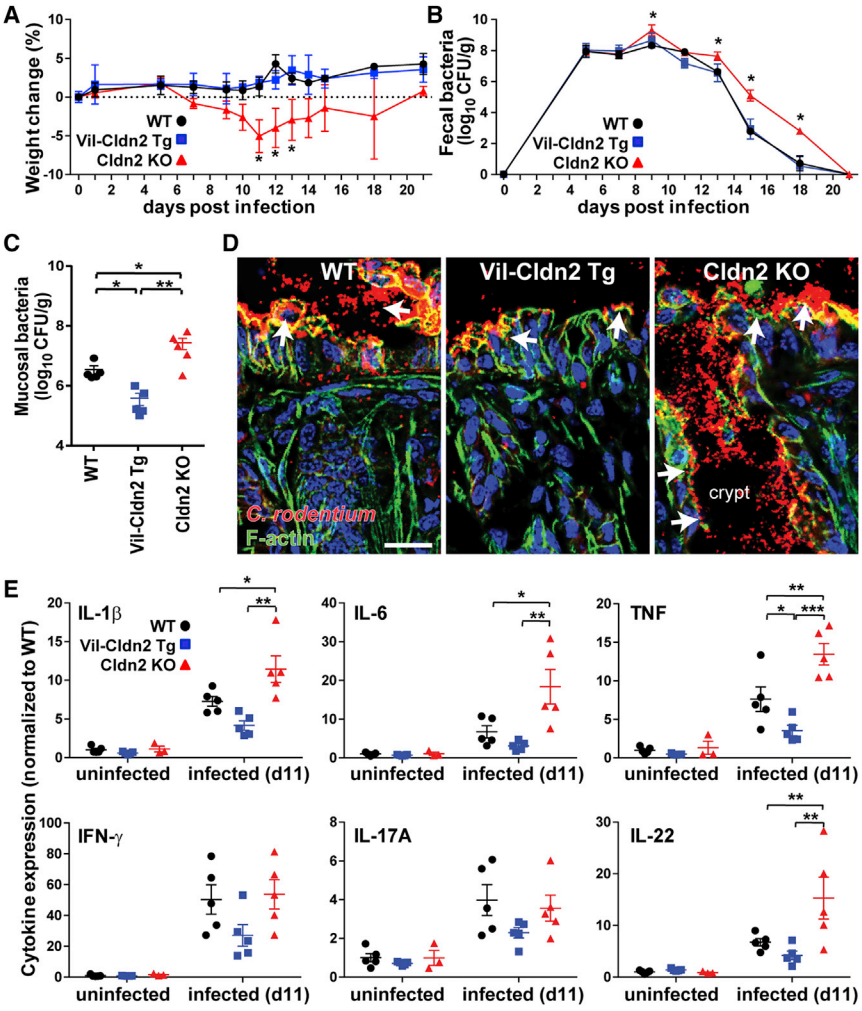

Figure 4. Claudin-2 Promotes *C. rodentium* Clearance and Limits Mucosal Immune Activation

(A) Weights of wild-type (WT), claudin-2 transgenic (Vil-Cldn2 Tg), and claudin-2 knockout (Cldn2 KO) mice during *C. rodentium* colitis (n = 7). Error bar represents mean ± SEM.

(B) Fecal *C. rodentium* in wild-type, claudin-2 transgenic, and claudin-2 knockout mice at indicated times after infection (n = 5). Error bar represents mean ± SEM. *p < 0.05.

(C) Mucosa-associated *C. rodentium* in wild-type, claudin-2 transgenic, and claudin-2 knockout mice 11 days after infection (n = 5 per condition). Error bar represents mean ± SEM. *p < 0.05, **p < 0.01.

(D) Immunofluorescent microscopy of *C. rodentium* (red), F-actin (green), DNA (blue) 11 days after infection. Crypt spaces were only colonized in claudin-2 knockout mice (p < 0.05). Scale bar represents 50 μm.

(E) Mucosal cytokine content in wild-type, claudin-2 transgenic, and claudin-2 knockout mice before and 11 days after *C. rodentium* infection (n = 5). Error bar represents mean ± SEM. *p < 0.05, **p < 0.01, ***p < 0.001.

proportional, such that the ratios of creatinine and 4 kDa dextran permeabilities to 70 kDa dextran permeability were unchanged (Figure 5D). This indicates that the increased absolute permeabilities observed reflect increased flux across the unrestricted, i.e., epithelial damage, pathway. The greater permeability increases in claudin-2 knockout mice are therefore indicative of severe mucosal damage, consistent with the analyses of histopathology, apoptosis, and compensatory proliferation.

As shown in Figure 3, fecal water content of uninfected claudin-2 transgenic mice was greater than that of uninfected wild-type or claudin-2 knockout mice (Figure 5E). However, fecal water content of claudin-2 transgenic and wild-type mice was similar beginning at day of infection, consistent with the kinetics of claudin-2 upregulation in wild-type mice. More strikingly, fecal water content in claudin-2 knockout mice increased dramatically at day 11 and remained significantly greater than that of both wild-type and claudin-2 transgenic mice until day 21 (Figure 5E). The increase in fecal water coincided with the peak of disease in claudin-2 knockout mice and correlated with the markedly greater tissue damage experienced by these mice at that time. As a whole, the analyses of apoptosis, histopathology, permeability, and fecal water content therefore indicate that increased fecal water from days 11 to 18 in claudin-2 knockout mice was secondary to increased unrestricted pathway permeability. These results indicate that increased intestinal epithelial claudin-2 expression is an important host defense response that limits *C. rodentium*-induced intestinal pathology. The data further suggest that, in the absence of pore pathway water efflux, increased unrestricted pathway permeability allows diarrhea to develop. The temporal correlation between increased fecal water and bacterial shedding in claudin-2 knockout mice further indicates that diarrhea resulting from water efflux is critical to pathogen clearance.

Osmotically Driven Water Efflux Rescues Claudin-2 Knockout Mice from Severe Infectious Colitis

As noted above, claudin-2 forms a paracellular channel that conducts Na^+ and water. We therefore hypothesized that the protection against *C. rodentium* colitis observed in wild-type and claudin-2 transgenic, relative to claudin-2 knockout, mice might simply be due to increased paracellular water efflux. To test this idea without expressing claudin-2, mice received polyethylene glycol (PEG) in their drinking water. PEG is a nontoxic, nonabsorbable molecule that, due to its osmotic activity within the lumen, draws fluid across the paracellular space and induces diarrhea. This approach is used routinely in patients in order to cleanse the bowel prior to colonoscopy.

The bowel-preparation solutions used to induce diarrhea in patients generally contain low molecular mass, 3.35 kDa PEG, at 6% (w/v). Preliminary studies showed that administration of low molecular mass PEG at a much lower dose (2%) was insufficient to cause diarrhea in mice but did increase fecal water content to a level similar to that in uninfected claudin-2

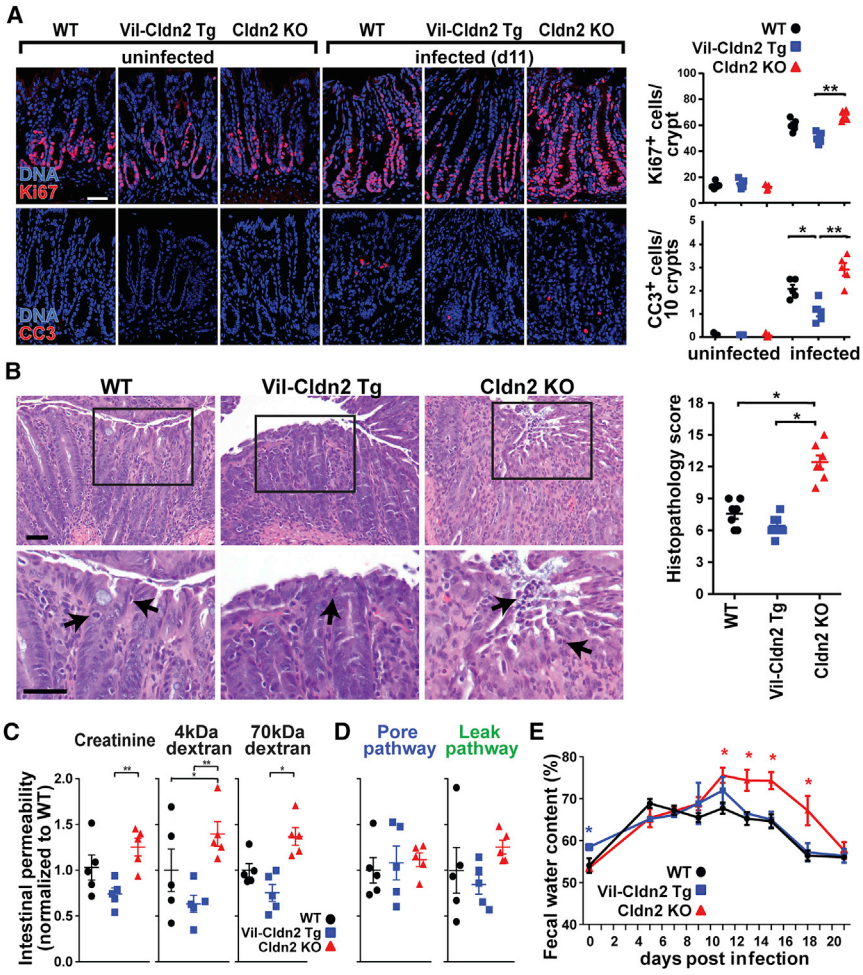

Figure 5. Claudin-2 Upregulation Limits *C. rodentium*-Induced Tissue Damage

(A) Epithelial proliferative and apoptotic responses at day 11 of *C. rodentium* infection. Ki67 (red), cleaved caspase-3 (CC3, red), DNA (blue), (n = 5). Scale bar represents 50 μm. Error bar represents mean ± SEM. *p < 0.05, **p < 0.01.

(B) Colonic histopathology at day 11 of *C. rodentium* infection (n = 7). Scale bar represents 50 μm. Error bar represents mean ± SEM. *p < 0.05.

(C) Creatinine, 4 kDa dextran, and 70 kDa dextran permeabilities on day 11 of infection. Data shown are normalized to means of infected wild-type mice (n = 5). Error bar represents mean ± SEM. *p < 0.05, **p < 0.01.

(D) Ratiometric analyses of specific pore (creatinine/70 kDa dextran) and leak (40 kDa dextran/70 kDa dextran) pathway permeabilities (n = 5). Error bar represents mean ± SEM.

(E) Fecal water content during *C. rodentium* infection (n = 5). Error bar represents mean ± SEM. *p < 0.05.

transgenic mice when given continuously for 7 days (Figure S2). Importantly, PEG treatment did not alter expression of claudin-2 or other tight junction proteins (Figure S3).

Treatment with PEG for 7 days, beginning at day 4 of infection (Figure 6A) significantly reduced numbers of mucosa-associated *C. rodentium* in wild-type and claudin-2 knockout mice (Figure 6B). In contrast, PEG did not reduce mucosa-associated *C. rodentium* numbers in claudin-2 transgenic mice (Figure 6B). This was expected, as water efflux is increased in claudin-2 transgenic mice even in the absence of PEG treatment. The data, therefore, support the conclusion that the PEG-induced water efflux maximizes pathogen clearance in wild-type and claudin-2 knockout mice. These results also suggest that pathogen clearance was maximized by transgenic claudin-2 expression and could not be enhanced further. Consistent with this, PEG treatment eliminated genotype-dependent differences in fecal *C. rodentium* shedding (Figure 6C).

Although a previous study reported that 5% PEG reduced *C. rodentium* attachment to cultured colonic epithelial monolayers by downregulating β_1-integrin (Qi et al., 2011), PEG did not affect intestinal epithelial β_1-integrin expression in vivo (Figure S4). Moreover, as treatment was not initiated until 4 days after infection, PEG would not be expected to affect initial bacterial adherence in the experiments shown here. We also considered the possibility that PEG might interfere with *C. rodentium* growth, but this was excluded by in vitro analyses of bacterial growth (Figure S5) as well as the failure of PEG to reduce fecal *C. rodentium* numbers in wild-type or claudin-2 transgenic mice (Figure 6C).

Morphologically, PEG prevented *C. rodentium* from colonizing colonic crypts in claudin-2 knockout mice, although surface colonization persisted (Figure 6D, arrows). Finally, PEG significantly diminished mucosal IL-1β, IL-6, TNF, IFN-γ, and IL-22 mucosal cytokine content in claudin-2 knockout, but not wild-type or claudin-2 transgenic, mice (Figure 6E). In contrast, PEG had no effect on mucosal cytokine expression in uninfected mice (Figure S6). These data suggest that, by increasing water efflux and promoting pathogen clearance, claudin-2 or PEG provide negative feedback that limits IL-22 production. PEG-induced water efflux therefore promotes *C. rodentium* clearance and limits mucosal immune activation in a manner similar to claudin-2 upregulation.

Osmotic Diarrhea Limits Barrier Loss, Epithelial Apoptosis, and Tissue Damage

PEG treatment of uninfected mice had no effect on creatinine, 4 kDa dextran, or 70 kDa dextran permeabilities (Figure S7). In contrast, PEG markedly reduced infection-associated increases in creatinine (Figure 7A), 4 kDa dextran (Figure 7B), and 70 kDa dextran (Figure 7C) permeabilities in claudin-2 knockout mice and had more modest effects on wild-type mice. The magnitudes to which PEG limited infection-induced permeability increases in wild-type and claudin-2 knockout mice were proportional for all probes, including 70 kDa dextran. This effect of PEG must therefore reflect reduced tissue damage, i.e., decreased unrestricted pathway flux, as that is the only route that accommodates 70 kDa dextran. Consistent with their increased basal fecal water

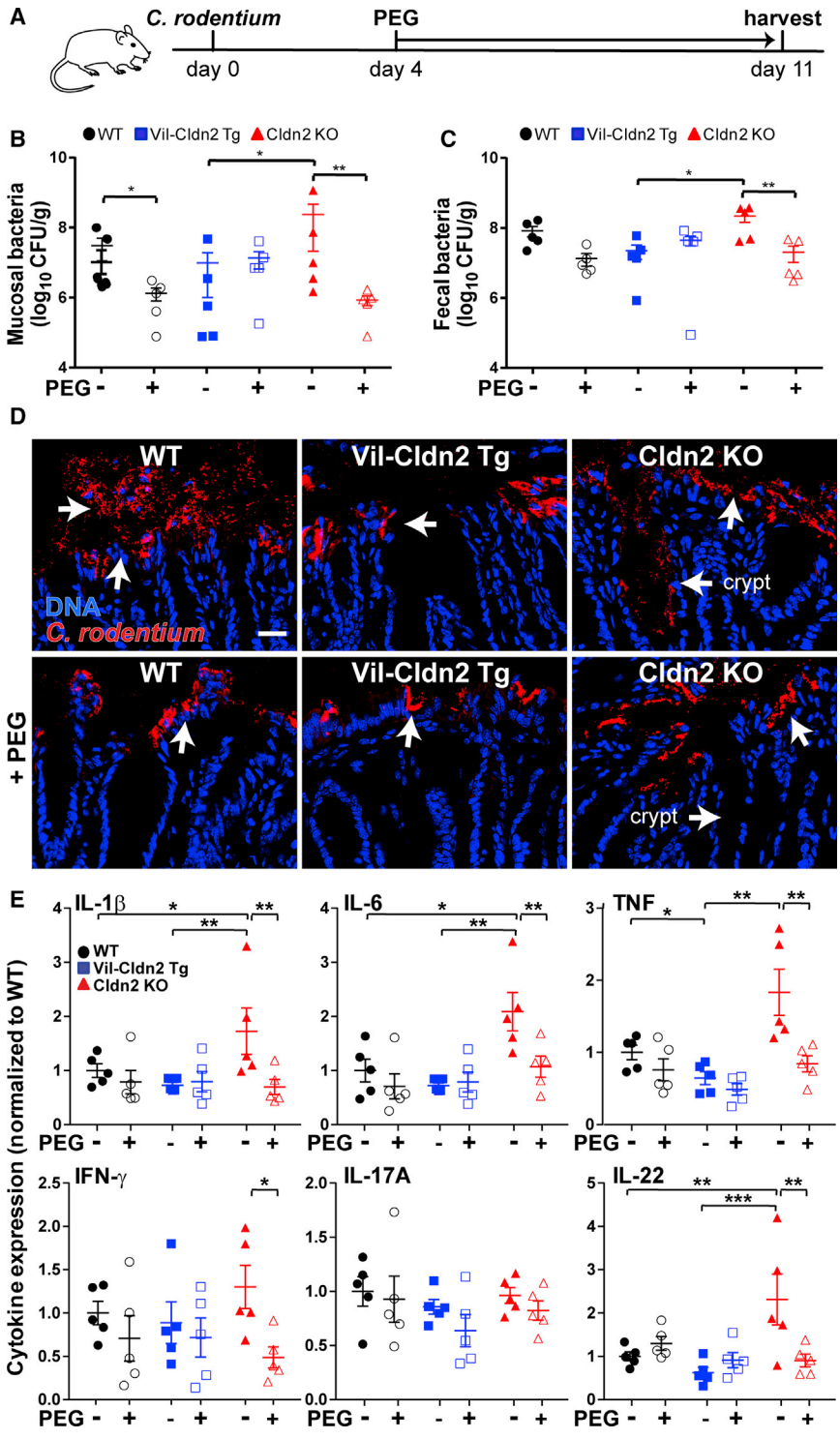

Figure 6. Osmotic Diarrhea Reduces Bacterial Colonization and Mucosal Immune Responses Induced by *C. rodentium* Infection

(A) Schematic of infection and PEG treatment.

(B) Mucosa-associated *C. rodentium* numbers in wild-type (WT), claudin-2 transgenic (Vil-Cldn2 Tg), and claudin-2 knockout (Cldn2 KO) mice at day 11 (n = 5). Error bar represents mean ± SEM. *p < 0.05, **p < 0.01.

(C) Fecal *C. rodentium* at day 11 after infection (n = 5). Error bar represents mean ± SEM. *p < 0.05, **p < 0.01.

(D) Immunofluorescent microscopy of *C. rodentium* (red) and DNA (blue) 11 days after infection. Colonization of crypt spaces in claudin-2 knockout mice is blocked by PEG treatment (p < 0.05). Scale bar represents 50 μm.

(E) Mucosal cytokines on day 11 of infection (n = 5). Error bar represents mean ± SEM. *p < 0.05, **p < 0.01, ***p < 0.001.

content, claudin-2 transgenic mice did not benefit from PEG treatment (Figures 7A–7C). Creatinine, 4 kDa dextran, and 70 kDa dextran permeabilities were therefore similar in *C. rodentium*-infected, PEG-treated mice regardless of genotype.

Epithelial apoptosis is characteristic of *C. rodentium* infection and is further increased in claudin-2 knockout mice (Figure 4B). PEG treatment reduced apoptotic frequency in both wild-type and claudin-2 knockout mice (Figure 7D) and was mirrored by reductions in epithelial proliferation (Figure 7E). As with *C. rodentium* colonization, cytokine production, and probe permeability, PEG reduced fecal water content in claudin-2 knockout and wild-type mice at day 11 (Figure 7F), when water efflux is primarily mediated by the unrestricted pathway. Consistent with these benefits, PEG treatment reduced histopathology in claudin-2 knockout mice (Figures 7G and 7H). Taken together, these results demonstrate that the impaired *C. rodentium* clearance and more severe disease observed in claudin-2 knockout mice are due to reduced paracellular water transport and can be largely reversed by induction of an osmotic diarrhea that draws water into the gut lumen by claudin-2-independent mechanisms.

DISCUSSION

The hypothesis that diarrhea clears enteric pathogens has been debated for centuries (Davison, 1922). Data supporting this idea are limited to the observation that antimotility agents, which can lessen diarrhea severity, can also delay pathogen clearance (DuPont and Hornick, 1973). Nevertheless, support for the idea that diarrhea is beneficial is weak, and, despite limited evidence of efficacy in most infections, efforts to develop therapeutic ion channel modulators that may prevent diarrhea continue. We sought to define the role of diarrhea in pathogen clearance using the model A/E pathogen *C. rodentium*.

Infection by A/E pathogens results in intestinal barrier loss due to tight junction dysregulation and epithelial damage. Here, we

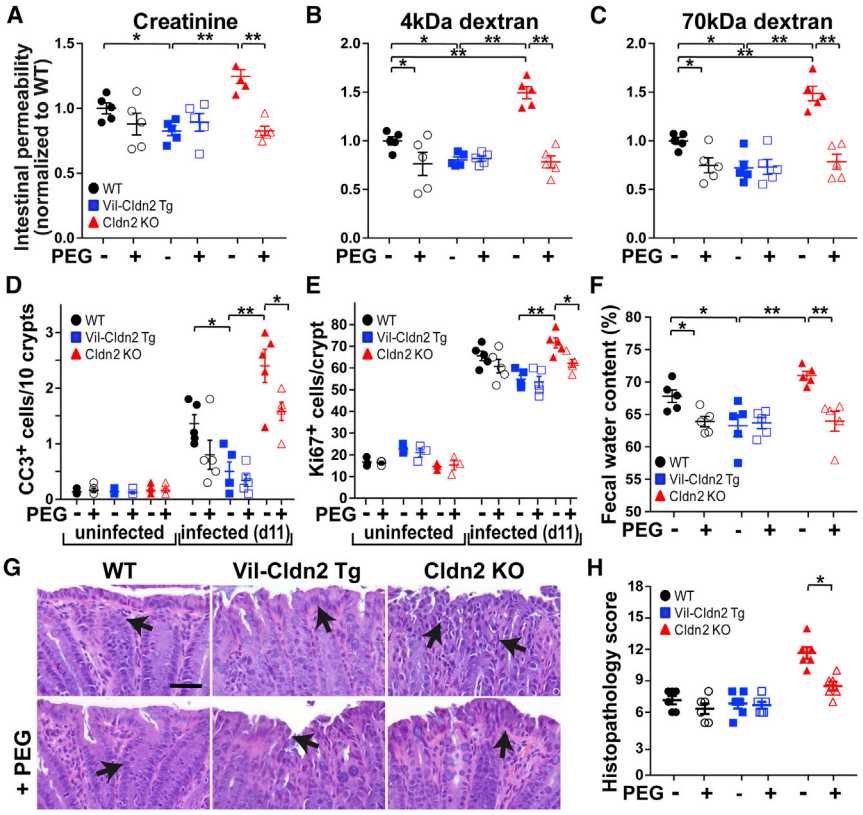

Figure 7. Osmotic Diarrhea Protects Claudin-2 Knockout Mice from Severe *C. rodentium* Colitis

(A–C) Creatinine (A), 4 kDa dextran (B), and 70 kDa dextran (C) permeabilities in wild-type (WT), claudin-2 transgenic (Vil-Cldn2 Tg), and claudin-2 knockout (Cldn2 KO) mice on day 11 after infection (n = 5). Error bar represents mean ± SEM. *p < 0.05, **p < 0.01.

(D) Epithelial apoptosis as detected by cleaved caspase-3 (CC3) staining on day 11 after infection (n = 5). Error bar represents mean ± SEM. *p < 0.05, **p < 0.01.

(E) Epithelial proliferation as detected by Ki67 staining on day 11 after infection (n = 5). Error bar represents mean ± SEM. *p < 0.05, **p < 0.01.

(F) Fecal water on day 11 after infection (n = 5). Error bar represents mean ± SEM. *p < 0.05, **p < 0.01.

(G and H) Representative histopathology images (G) and scores (H) in *C. rodentium* infection (n = 5). Arrows indicate neutrophils. Scale bar represents 50 μm. Error bar represents mean ± SEM. *p < 0.05, **p < 0.01.

developed an assay that allows size-specific analysis of intestinal permeability and dissection of three distinct modes of barrier loss during *C. rodentium* infection. The results indicate that, within 2 days of infection, before morphological features of inflammation or tissue damage have developed, IL-22-dependent signaling promotes colonic epithelial claudin-2 expression that enhances permeability of small probes, e.g., creatinine, but not more commonly used larger probes such as 4 kDa dextran. The increased fecal water induced by transgenic claudin-2 expression in uninfected mice provides further evidence that inflammation and epithelial damage are not required for the permeability increases or diarrhea that develop during infection. Claudin-2-dependent water efflux does, however, promote pathogen clearance and limit disease severity. Whether these claudin-2-dependent increases in water efflux simply wash away adherent *C. rodentium* or, alternatively, have some other effects on the microbiome has not been addressed here but could be an interesting question. Regardless of the mechanism, the claudin-2-dependent pathogen clearance described here is distinct from IL-13-dependent helminth expulsion, where claudin-2 upregulation occurs but does not contribute significantly to host defense (Sun et al., 2016).

The data presented here show that IL-22 is required for claudin-2 upregulation in vivo. In vitro studies indicate that claudin-2 upregulation depends on STAT3 and STAT6 signaling (Rosen et al., 2013; Weber et al., 2010). Separate studies have shown that epithelial STAT3 signaling is essential for effects of IL-22 on epithelial homeostasis and repair during acute colitis (Pickert et al., 2009). Available data therefore indicate that IL-22 upregulates epithelial STAT signaling in vivo and that STAT signaling is required for epithelial claudin-2 upregulation in vitro. By demonstrating that IL-22 signaling is necessary and sufficient to drive epithelial claudin-2 upregulation in *C. rodentium* infection, these data link the previous observations and lead to the conclusion that IL-22-mediated claudin-2 expression occurs via a STAT-dependent process. Although IL-22 has not been previously recognized as a regulator of claudin-2 expression, other effects of IL-22-dependent epithelial STAT3 signaling, such as inhibition of enteric viral infection, might also reflect claudin-2 upregulation (Xue et al., 2017). Thus, claudin-2-mediated water efflux may be a widely used mechanism of innate defense.

Our data indicate that diarrhea, whether driven by claudin-2-mediated paracellular Na^+ and water flux or an osmotic agent, promotes pathogen clearance. Although not tested in vivo, in vitro studies suggest that increased water flux driven by other means, such as chloride secretion induced by activation of apical chloride channels, could have similar effects (Keely et al., 2012). Water efflux might also occur via transcellular, rather than paracellular, transport. Consistent with this idea, epithelial aquaporin-4 expression has been reported to be enhanced by IL-22 signaling (Pham et al., 2014). However, most studies have failed to identify a role for aquaporins in intestinal water transport, and recent data suggest that intestinal epithelial aquaporins are more important for transport of bioactive signaling molecules, such as H_2O_2, than water (Thiagarajah et al., 2017; Yang et al., 2005). Thus, despite the potential involvement of many processes, including several activated by IL-22, in triggering the water efflux that enhances bacterial clearance, claudin-2 upregulation is the primary mechanism employed in *C. rodentium* colitis.

In addition to promoting pathogen clearance, the diarrhea driven by claudin-2 expression limited epithelial apoptosis and the associated repair response. Epithelial proliferation and

apoptosis were not, however, affected by claudin-2 knockout or transgene expression in the absence of challenge. This contrasts with the increased colonic epithelial proliferation reported in a different claudin-2 transgenic mouse (Ahmad et al., 2014). Given the absence of mucosal hypertrophy in that mouse, one can conclude that the previously reported claudin-2 transgenic mouse suffered from chronic, low-grade epithelial damage. The absence of this phenotype in the claudin-2 transgenic mouse reported here indicates that the damage is not a direct result of increased claudin-2 expression. Further, our data suggest that increased fecal water content and resulting DSS dilution may be a simple explanation for the DSS-resistant phenotype of the previously reported claudin-2 transgenic mice (Ahmad et al., 2014). Given the increased claudin-2 expression that normally occurs during DSS colitis, this hypothesis is also consistent with the enhanced DSS colitis severity described in claudin-2 knockout mice (Nishida et al., 2013).

Multiple immune cell subsets produce IL-22 during *C. rodentium* infection (Basu et al., 2012; Rankin et al., 2016). This IL-22 production requires epithelial NFκB signaling (Giacomin et al., 2015), thereby explaining how a noninvasive pathogen can activate subepithelial immune cells. Previous studies have shown that intestinal epithelial IL-22RA signaling contributes to host defense during *C. rodentium* infection and that intestinal epithelial IL-22RA knockout results in exaggerated mucosal IL-22 production (Pham et al., 2014). This is remarkably similar to the effects of claudin-2 knockout and supports the hypothesis that IL-22-dependent claudin-2 upregulation feeds back to limit IL-22 production.

In sum, the results presented here indicate that innate immune activation and IL-22-dependent increases in claudin-2 expression and pore pathway paracellular permeability are essential to host defense. This suggests that, while inhibition of permeability increases might limit diarrhea in early stages of infection, this intervention may also delay pathogen clearance and prolong disease. Thus, while therapeutic claudin-2 inhibition has been proposed, it may be contraindicated in infectious enterocolitis. As a whole, our studies provide direct evidence that increased tight junction permeability and the diarrhea that follows are critical to enteric pathogen clearance and define these as a previously unrecognized contribution of IL-22 to host defense.

STAR★METHODS

Detailed methods are provided in the online version of this paper and include the following:

- KEY RESOURCES TABLE
- CONTACT FOR REAGENT AND RESOURCE SHARING
- EXPERIMENTAL MODEL AND SUBJECT DETAILS
  - Mice
- METHOD DETAILS
  - Epithelial Cell Isolation
  - Primary Cell Culture and Cytokine Stimulation
  - *Citrobacter rodentium* Infection
  - *Citrobacter rodentium* Quantification
  - Cytokine and Antibody Treatment
  - Intestinal Permeability Assay
  - Fecal Na^+ and Water Determination
  - RNA Isolation and Quantitative Real-Time RT-PCR
  - ELISA
  - Western Blots
  - Immunofluorescence Staining and Microscopy
  - Histopathological Scoring
  - Quantification and Statistical Analysis

SUPPLEMENTAL INFORMATION

Supplemental Information includes seven figures and one table and can be found with this article online at http://dx.doi.org/10.1016/j.chom.2017.05.009.

AUTHOR CONTRIBUTIONS

Conceptualization: P.-Y.T., B.K.Z., Y.X.F., and J.R.T; Methodology: P.-Y.T., B.K.Z., M.A.W., L.S., Y.-X.F., and J.R.T.; Investigation: P.-Y.T., B.K.Z., W.-Q.H., J.-M.Z., M.A.O., G.S., A.S., S.Y., W.-T.K., and J.R.T.; Resources: A.T., Y.-X.F., and S.T.; Writing – original draft preparation: P.-Y.T. and J.R.T.; Writing – review and editing: P.-Y.T., B.K.Z., and J.R.T. with input from all other authors; Supervision: J.R.T.; Funding acquisition: J.R.T., B.K.Z., M.A.O., and S.T.

ACKNOWLEDGMENTS

We are grateful to Natalie Ronaghan, Tiffany S. DaVanzo, Edda Fiebiger, and Richard S. Blumberg for their conceptual and technical contributions. This work was supported by National Institute of Health grants F30DK103511 (M.A.O.), T32HD007009 (M.A.O.), R01DK61931 (J.R.T.), R01DK68271 (J.R.T.), and R24DK099803 (J.R.T.); a Senior Research Award from the Crohn's and Colitis Foundation (J.R.T.); and the State Scholarship Fund of China 201208110294 (B.K.Z.); and Core Research for Evolutional Science and Technology of the Japan Science and Technology Agency (S.T.).

Received: March 28, 2017
Revised: May 8, 2017
Accepted: May 25, 2017
Published: June 14, 2017

REFERENCES

Ahmad, R., Chaturvedi, R., Olivares-Villagómez, D., Habib, T., Asim, M., Shivesh, P., Polk, D.B., Wilson, K.T., Washington, M.K., Van Kaer, L., et al. (2014). Targeted colonic claudin-2 expression renders resistance to epithelial injury, induces immune suppression, and protects from colitis. Mucosal Immunol. *7*, 1340–1353.

Anderson, J.M., and Van Itallie, C.M. (2009). Physiology and function of the tight junction. Cold Spring Harb. Perspect. Biol. *1*, a002584.

Basu, R., O'Quinn, D.B., Silberger, D.J., Schoeb, T.R., Fouser, L., Ouyang, W., Hatton, R.D., and Weaver, C.T. (2012). Th22 cells are an important source of IL-22 for host protection against enteropathogenic bacteria. Immunity *37*, 1061–1075.

Clayburgh, D.R., Barrett, T.A., Tang, Y., Meddings, J.B., Van Eldik, L.J., Watterson, D.M., Clarke, L.L., Mrsny, R.J., and Turner, J.R. (2005). Epithelial myosin light chain kinase-dependent barrier dysfunction mediates T cell activation-induced diarrhea in vivo. J. Clin. Invest. *115*, 2702–2715.

Davison, W.C. (1922). A bacteriological and clinical consideration of bacillary dysentery in adults and children. Medicine *1*, 389–510.

Deng, W., de Hoog, C.L., Yu, H.B., Li, Y., Croxen, M.A., Thomas, N.A., Puente, J.L., Foster, L.J., and Finlay, B.B. (2010). A comprehensive proteomic analysis of the type III secretome of Citrobacter rodentium. J. Biol. Chem. *285*, 6790–6800.

DuPont, H.L., and Hornick, R.B. (1973). Adverse effect of lomotil therapy in shigellosis. JAMA *226*, 1525–1528.

Giacomin, P.R., Moy, R.H., Noti, M., Osborne, L.C., Siracusa, M.C., Alenghat, T., Liu, B., McCorkell, K.A., Troy, A.E., Rak, G.D., et al. (2015). Epithelial-intrinsic IKKα expression regulates group 3 innate lymphoid cell responses and antibacterial immunity. J. Exp. Med. *212*, 1513–1528.

Guttman, J.A., Li, Y., Wickham, M.E., Deng, W., Vogl, A.W., and Finlay, B.B. (2006). Attaching and effacing pathogen-induced tight junction disruption in vivo. Cell. Microbiol. *8*, 634–645.

Holmes, J.L., Van Itallie, C.M., Rasmussen, J.E., and Anderson, J.M. (2006). Claudin profiling in the mouse during postnatal intestinal development and along the gastrointestinal tract reveals complex expression patterns. Gene Expr. Patterns *6*, 581–588.

Keely, S., Kelly, C.J., Weissmueller, T., Burgess, A., Wagner, B.D., Robertson, C.E., Harris, J.K., and Colgan, S.P. (2012). Activated fluid transport regulates bacterial-epithelial interactions and significantly shifts the murine colonic microbiome. Gut Microbes *3*, 250–260.

Mankertz, J., Amasheh, M., Krug, S.M., Fromm, A., Amasheh, S., Hillenbrand, B., Tavalali, S., Fromm, M., and Schulzke, J.D. (2009). TNFalpha up-regulates claudin-2 expression in epithelial HT-29/B6 cells via phosphatidylinositol-3-kinase signaling. Cell Tissue Res. *336*, 67–77.

Nik, A.M., and Carlsson, P. (2013). Separation of intact intestinal epithelium from mesenchyme. Biotechniques *55*, 42–44.

Nishida, M., Yoshida, M., Nishiumi, S., Furuse, M., and Azuma, T. (2013). Claudin-2 regulates colorectal inflammation via myosin light chain kinase-dependent signaling. Dig. Dis. Sci. *58*, 1546–1559.

Pham, T.A., Clare, S., Goulding, D., Arasteh, J.M., Stares, M.D., Browne, H.P., Keane, J.A., Page, A.J., Kumasaka, N., Kane, L., et al.; Sanger Mouse Genetics Project (2014). Epithelial IL-22RA1-mediated fucosylation promotes intestinal colonization resistance to an opportunistic pathogen. Cell Host Microbe *16*, 504–516.

Pickert, G., Neufert, C., Leppkes, M., Zheng, Y., Wittkopf, N., Warntjen, M., Lehr, H.A., Hirth, S., Weigmann, B., Wirtz, S., et al. (2009). STAT3 links IL-22 signaling in intestinal epithelial cells to mucosal wound healing. J. Exp. Med. *206*, 1465–1472.

Pinto, D., Robine, S., Jaisser, F., El Marjou, F.E., and Louvard, D. (1999). Regulatory sequences of the mouse villin gene that efficiently drive transgenic expression in immature and differentiated epithelial cells of small and large intestines. J. Biol. Chem. *274*, 6476–6482.

Qi, W., Joshi, S., Weber, C.R., Wali, R.K., Roy, H.K., and Savkovic, S.D. (2011). Polyethylene glycol diminishes pathological effects of Citrobacter rodentium infection by blocking bacterial attachment to the colonic epithelia. Gut Microbes *2*, 267–273.

Raleigh, D.R., Boe, D.M., Yu, D., Weber, C.R., Marchiando, A.M., Bradford, E.M., Wang, Y., Wu, L., Schneeberger, E.E., Shen, L., and Turner, J.R. (2011). Occludin S408 phosphorylation regulates tight junction protein interactions and barrier function. J. Cell Biol. *193*, 565–582.

Rankin, L.C., Girard-Madoux, M.J., Seillet, C., Mielke, L.A., Kerdiles, Y., Fenis, A., Wieduwild, E., Putoczki, T., Mondot, S., Lantz, O., et al. (2016). Complementarity and redundancy of IL-22-producing innate lymphoid cells. Nat. Immunol. *17*, 179–186.

Rosen, M.J., Chaturvedi, R., Washington, M.K., Kuhnhein, L.A., Moore, P.D., Coggeshall, S.S., McDonough, E.M., Weitkamp, J.H., Singh, A.B., Coburn, L.A., et al. (2013). STAT6 deficiency ameliorates severity of oxazolone colitis by decreasing expression of claudin-2 and Th2-inducing cytokines. J. Immunol. *190*, 1849–1858.

Rosenthal, R., Günzel, D., Krug, S.M., Schulzke, J.D., Fromm, M., and Yu, A.S. (2017). Claudin-2-mediated cation and water transport share a common pore. Acta Physiol. (Oxf.) *219*, 521–536.

Sato, T., Stange, D.E., Ferrante, M., Vries, R.G., Van Es, J.H., Van den Brink, S., Van Houdt, W.J., Pronk, A., Van Gorp, J., Siersema, P.D., and Clevers, H. (2011). Long-term expansion of epithelial organoids from human colon, adenoma, adenocarcinoma, and Barrett's epithelium. Gastroenterology *141*, 1762–1772.

Sun, R., Urban, J.F., Jr., Notari, L., Vanuytsel, T., Madden, K.B., Bohl, J.A., Ramalingam, T.R., Wynn, T.A., Zhao, A., and Shea-Donohue, T. (2016). Interleukin-13 receptor α1-dependent responses in the intestine are critical to parasite clearance. Infect. Immun. *84*, 1032–1044.

Suzuki, T., Yoshinaga, N., and Tanabe, S. (2011). Interleukin-6 (IL-6) regulates claudin-2 expression and tight junction permeability in intestinal epithelium. J. Biol. Chem. *286*, 31263–31271.

Thiagarajah, J.R., Chang, J., Goettel, J.A., Verkman, A.S., and Lencer, W.I. (2017). Aquaporin-3 mediates hydrogen peroxide-dependent responses to environmental stress in colonic epithelia. Proc. Natl. Acad. Sci. USA *114*, 568–573.

Turner, J.R. (2009). Intestinal mucosal barrier function in health and disease. Nat. Rev. Immunol. *9*, 799–809.

Wada, M., Tamura, A., Takahashi, N., and Tsukita, S. (2013). Loss of claudins 2 and 15 from mice causes defects in paracellular Na+ flow and nutrient transport in gut and leads to death from malnutrition. Gastroenterology *144*, 369–380.

Weber, C.R., Raleigh, D.R., Su, L., Shen, L., Sullivan, E.A., Wang, Y., and Turner, J.R. (2010). Epithelial myosin light chain kinase activation induces mucosal interleukin-13 expression to alter tight junction ion selectivity. J. Biol. Chem. *285*, 12037–12046.

Xue, M., Zhao, J., Ying, L., Fu, F., Li, L., Ma, Y., Shi, H., Zhang, J., Feng, L., and Liu, P. (2017). IL-22 suppresses the infection of porcine enteric coronaviruses and rotavirus by activating STAT3 signal pathway. Antiviral Res. *142*, 68–75.

Yang, B., Song, Y., Zhao, D., and Verkman, A.S. (2005). Phenotype analysis of aquaporin-8 null mice. Am. J. Physiol. Cell Physiol. *288*, C1161–C1170.

Zheng, Y., Valdez, P.A., Danilenko, D.M., Hu, Y., Sa, S.M., Gong, Q., Abbas, A.R., Modrusan, Z., Ghilardi, N., de Sauvage, F.J., and Ouyang, W. (2008). Interleukin-22 mediates early host defense against attaching and effacing bacterial pathogens. Nat. Med. *14*, 282–289.

STAR★METHODS

KEY RESOURCES TABLE

REAGENT or RESOURCE	SOURCE	IDENTIFIER
Antibodies		
Rabbit polyclonal anti-claudin-2 (ab53032)	Abcam	RRID: AB_869174
Rabbit polyclonal anti-claudin-15 (38-9200)	ThermoFisher	RRID: AB_2533391
Rabbit polyclonal anti-*Citrobacter koseri* (ab37056)	Abcam	RRID: AB_726896
Rabbit polyclonal anti-Ki67 (ab15580)	Abcam	RRID: AB_443209
Rabbit monoclonal anti-cleaved caspase-3 (9664)	Cell Signaling Technology	RRID: AB_2070042
Rabbit monoclonal anti-E-cadherin (3195)	Cell Signaling Technology	RRID: AB_2291471
Mouse monoclonal anti-E-cadherin (76055)	Abcam	RRID: AB_1310159
Mouse monoclonal anti-β actin (A1978)	Sigma-Aldrich	RRID: AB_476692
Goat anti-rabbit IgG (H+L), HRP conjugate (7074)	Cell Signaling Technology	RRID: AB_2099233
Horse anti-mouse IgG (H+L), HRP conjugate (7076)	Cell Signaling Technology	RRID: AB_330924
Donkey anti-rabbit IgG (H+L), Alexa 594 conjugate, highly cross-adsorbed $F(ab')_2$ fragments (711-586-152)	Jackson ImmunoResearch	RRID: AB_2340622
Donkey anti-mouse IgG (H+L), Alexa 488 conjugate, highly cross-adsorbed $F(ab')_2$ fragments (715-546-151)	Jackson ImmunoResearch	RRID: AB_2340850
IRDye 800CW Goat anti-rabbit IgG (H+L) (925-32211)	LI-COR Biosciences	RRID: AB_2651127
IRDye 680RD Goat anti-Mouse IgG (H+L) (925-68070)	LI-COR Biosciences	RRID: AB_2651128
Monoclonal anti-IL-22 neutralizing antibody (IgG1, clone 8E11.9)	Genentech	RRID: AB_2651129
Mouse anti-OVA control antibody (IgG1, clone F2-3.58)	BioXCell	RRID: AB_2651130
Bacterial and Virus Strains		
Citrobacter rodentium (strain DBS100)	ATCC	Cat#ATCC51459
Biological Samples		
Organoids were derived from isolated intestinal epithelium of 8-10 week old C57BL/6J mice	N/A	N/A
Epithelial cells isolated from distal colon of 8-10 week old C57BL/6J, claudin-2 knockout/C57BL/6J, or claudin-2 transgenic/C57BL/6J mice; all were bred on-site as cage- or litter-mates	N/A	N/A
Chemicals, Peptides, and Recombinant Proteins		
Recombinant murine IL-1β (211-11B)	PeproTech	N/A
Recombinant murine IL-6 (216-16)	PeproTech	N/A
Recombinant murine IL-17 (210-17)	PeproTech	N/A
Recombinant murine IL-22 (210-22)	PeproTech	N/A
Recombinant murine TNF (315-01A)	PeproTech	N/A
Recombinant murine IFN-γ (315-05)	PeproTech	N/A
Matrigel (356234)	Corning	N/A
Cell Recovery Solution (354253)	Corning	N/A
Epidermal growth factor (315-09)	PeproTech	N/A
Noggin (250-38)	PeproTech	N/A
R-spondin (315-32)	PeproTech	N/A
Fluorescein isothiocyanate-4 kDa dextran (46944)	Sigma-Aldrich	N/A
Rhodamine B isothiocyanate-70 kDa dextran (R9379)	Sigma-Aldrich	N/A
Creatinine (C4255)	Sigma-Aldrich	N/A
MacConkey agar (M7408)	Sigma-Aldrich	N/A
Polyethylene glycol, MW 3,350 (P4338)	Sigma-Aldrich	N/A
Zirconia-silica beads, 0.1mm dia (11079101z)	Biospec	N/A

(*Continued on next page*)

Continued

REAGENT or RESOURCE	SOURCE	IDENTIFIER
Alexa Fluor 647 Phalloidin (A22287)	Invitrogen	N/A
Alexa Fluor 594 Phalloidin (A12381)	Invitrogen	N/A
Hoechst 33342 (H3570)	Invitrogen	N/A
Bio-Plex Cell Lysis Kit (171-304011)	Bio-Rad	N/A
Critical Commercial Assays		
RNeasy Mini Kit (74106)	QIAGEN	N/A
RNase-Free Dnase Set (79254)	QIAGEN	N/A
iScript cDN/A kit (1725038)	Bio-Rad	N/A
SsoFast EvaGreen supermixes (1725202)	Bio-Rad	N/A
Protein Assay Kit II (5000002)	Bio-Rad	N/A
Mouse IL-1β ELISA Ready-SET-Go! (88-7013-86)	eBioscience	N/A
Mouse IL-6 ELISA Ready-SET-Go! (88-7064-86)	eBioscience	N/A
Mouse IL-17 ELISA Ready-SET-Go! (88-7371-86)	eBioscience	N/A
Mouse IL-22 ELISA Ready-SET-Go! (88-7422-86)	eBioscience	N/A
Mouse TNF ELISA Ready-SET-Go! (88-7324-86)	eBioscience	N/A
Mouse IFN-γ ELISA Ready-SET-Go! (88-7314-88)	eBioscience	N/A
Mouse IL-10 ELISA Ready-SET-Go! (88-7137-86)	eBioscience	N/A
Mouse IL-13 ELISA Ready-SET-Go! (88-7105-86)	eBioscience	N/A
Oligonucleotides		
qPCR primers, see Table S1	This paper	N/A
Experimental Models: Organisms/Strains		
Mouse: C57BL/6J (000664)	The Jackson Laboratory	N/A
Mouse: claudin-2 knockout	Wada et al., 2013	N/A
Mouse: claudin-2 transgenic	This paper	N/A
Software and Algorithms		
MetaMorph 7.8	Molecular Devices	N/A
Autoquant X3	MediaCybernetics	N/A
ImageJ	NIH	N/A
GraphPad Prism 6.0	GraphPad Software	N/A
ImageStudio 5.0	LI-COR Biosciences	N/A
Microsoft Excel	Microsoft	N/A

CONTACT FOR REAGENT AND RESOURCE SHARING

Further information and requests for reagents should be directed to and will be fulfilled by the Lead Contact, Jerrold R Turner, MD, PhD (jrturner@bwh.harvard.edu).

EXPERIMENTAL MODEL AND SUBJECT DETAILS

Mice

C57BL/6 mice (Stock# 000664) were purchased from The Jackson Laboratory. Claudin-2 knockout mice on a C57BL/6 background were obtained from Dr. Sachiko Tsukita (Wada et al., 2013). A mammalian expression construct with the 9kB villin promoter (Pinto et al., 1999) followed by EGFP and mouse claudin-2 was injected into C57BL/6 embryos by the Transgenic Mouse and Embryonic Stem Cell Facility at the University of Chicago. Claudin-2 transgenic pups were born at expected Mendelian proportions, grew and gained weight identically to their littermates, and did not develop spontaneous disease. Preliminary experiments demonstrated that EGFP-claudin-2 was expressed, trafficked to the tight junction, and was functional. EGFP-claudin-2 expression was not detected in the kidney. Individual experiments were segregated, but all studies were performed in both sexes. Mice were bred under specific pathogen-free conditions and used at 6 – 8 weeks of age. Littermates or co-housed mice were used for all experiments. All studies were approved by the Animal Care and Use Committees of the University of Chicago, Brigham and Women's Hospital, and Boston Children's Hospital.

METHOD DETAILS

Epithelial Cell Isolation

Colonic epithelium were isolated using Cell Recovery Solution (Corning) as described (Nik and Carlsson, 2013). Briefly, colons were removed and flushed several times with ice-cold PBS. The tissue was inverted by inserting a gavage needle, securing the needle end with suture, and pulling the needle back. Following inversion, the other end of the inverted colon was secured with a suture. The gavage needle was then attached to a 1 mL syringe and the tissue was submerged in at 3 mL ice-cold Cell Recovery Solution in a FACS tube. The tissue was deflated and re-inflated with the plunger every 5 min for 30 min to recover epithelial sheets.

Primary Cell Culture and Cytokine Stimulation

For stem cell culture, intestinal epithelial cells were harvested from 8-10-week-old C57BL/6 mice and cultured in Matrigel (Corning) and fed with media containing epidermal growth factor, Noggin, and R-spondin, as previously described (Sato et al., 2011). Two days after splitting, organoid cultures were treated with recombinant murine IL-1β (10 ng/mL), IL-6 (50 ng/mL), IL-17 (10 ng/ml), IL-22 (10 ng/mL), TNF (10 ng/mL), or IFN-γ (10 ng/mL) for 48 hr. Cells were harvested from Matrigel using Cell Recovery Solution.

Citrobacter rodentium Infection

C. rodentium strain DBS100 (ATCC 51459; American Type Culture Collection) was grown in LB broth overnight with shaking at 37°C. Mice were fasted for 4 hr before oral inoculation of 2×10^9 colony-forming unit (CFU) *C. rodentium* in a volume of 0.2 mL sterile phosphate-buffered saline (PBS). Bacterial concentration was measured as absorbance at OD_{600} and confirmed independently for each experiment by serial dilution and growth on MacConkey agar.

For analysis of the effect of low molecular weight polyethylene glycol (PEG) on infection, filter-sterilized 2% PEG (MW 3,350) was added to the drinking water beginning on day 4 of *C. rodentium* infection.

Citrobacter rodentium Quantification

For analysis of *C. rodentium* shedding, feces were collected, weighed, homogenized in sterile PBS using with 0.1mm diameter zirconia-silica beads and a beadbeater (Biospec) for 20 s at room temperature. Mucosa-associated bacteria were assessed in 0.5 cm segments of distal colon that had been flushed with ice-cold sterile PBS to removal luminal contents and loosely adherent bacteria. Colonic segments were then weighed and homogenized identically to fecal samples. Serial dilutions of fecal and colonic homogenates were plated on MacConkey agar. *C. rodentium* were identified as pink colonies after 20 hr of growth at 37°C.

For analysis of the effect of PEG on bacterial growth, stationary phase cultures were diluted 1:100 into fresh LB media with or without 2% PEG and OD_{600} was measured at indicated intervals.

Cytokine and Antibody Treatment

Mice were injected i.p. with 5 μg recombinant murine IL-22 (PeproTech). Colonic epithelia were harvested after 24 hr. Mice were injected i.p. with 100 μg anti-IL-22 neutralizing or isotype-matched control monoclonal antibodies 48 hr prior to infection.

Intestinal Permeability Assay

Mice were denied access to food but allowed water for 3 hr prior to gavage with 0.2 mL saline containing 12 mg fluorescein isothiocyanate-4 kDa dextran, 8 mg rhodamine B isothiocyanate-70 kDa dextran, and 20 mg creatinine (Sigma). Serum was harvested after 5 hr. Creatinine was measured as described previously (Clayburgh et al., 2005). Recovery of creatinine and fluorescent probes was measured in a Synergy HT plate reader (BioTek) using freshly prepared standards. Fluorescence of fluorescein and rhodamine B were measured using excitation wavelengths of 495 nm and 555 nm and emission wavelengths of 525 nm and 585 nm, respectively.

Fecal Na^+ and Water Determination

Fresh stools were collected into pre-tared 1.5 mL tubes and immediately sealed. After weighing, tubes were uncapped and completely desiccated by incubation in a dry oven at 60°C for 24 hr. Tubes were then re-weighed, and fecal water was determined as the fraction of total mass lost upon desiccation. In order to provide sufficient sample for the Na^+ assay, dried stools were rehydrated with 5x the initial water volume and homogenized using a beadbeater, as above. After brief centrifugation to pellet insoluble debris, Na^+ content of the supernatant was measured using a B-722 LAQUAtwin Compact Sodium Ion Meter (Horiba). Fecal Na^+ mass was normalized to dry fecal mass.

RNA Isolation and Quantitative Real-Time RT-PCR

For qRT-PCR, total RNA was extracted using the RNeasy Mini Kit and on-column DNase I digestion (QIAGEN). cDNA synthesis was performed using the iScript cDNA kit (Bio-Rad). Real-time PCR used primers indicated (Table S1), and reactions were run using the SsoFast EvaGreen supermixes on a CFX96 thermocycler (Bio-Rad). Raw data were analyzed by the ΔCt method using the epithelial-specific gene keratin 8 for normalization. Changes were calculated by the ΔΔCt method.

ELISA

Portions of distal colon (0.5 cm) were washed using Bio-Plex wash buffer (Bio-Rad). and then homogenized in 0.5 mL Bio-Plex cell lysis buffer with 2mM PMSF using a sterile, 7 cm polypropylene pestle (Kimble). After freeze-thaw, samples were sonicated on ice, centrifuged for 5 min at 4,500 x *g*, and total protein within the supernatant was quantified using a Bradford protein assay (Bio-Rad). Supernatant (0.25 mg protein in 0.1 mL) was assayed for cytokines using Ready-SET-Go! ELISA kits (eBioscience).

Western Blots

Isolated epithelial cell and organoid lysates were separated by SDS-PAGE, transferred to PVDF membranes, and blotted using primary antibodies to claudin-2 (1:2,000 dilution, Abcam), claudin-15 (1:2,000 dilution, ThermoFisher), E-Cadherin (1:5,000 dilution, Cell Signaling Technologies), or β-actin (1:5,000 dilution, Sigma-Aldrich) overnight at 4°C. Membranes were then incubated with horseradish peroxidase (HRP)-conjugated or infrared dye-conjugated secondary antibodies for 1 hr at room temperature. Protein was detected using HyBlotCL film and quantified using ImageJ (HRP conjugates) or a LI-COR Odyssex Fc imager and quantified using ImageStudio (infrared conjugates).

Immunofluorescence Staining and Microscopy

Distal colons were snap-frozen as described previously (Clayburgh et al., 2005). Snap-frozen distal colons were incubated in 1% PFA in PBS for 10 min after cutting 5 μm sections. Sections were permeabilized with 0.5% NP-40 and blocked with 10% goat serum for 1 hr at room temperature. Sections were incubated with primary antibody diluted in PBS with 5% goat serum. Primary antibodies consisted of the same antibodies used for western blots or antibodies to *C. rodentium* (1:250 dilution, Abcam), Ki67 (1:250 dilution, Abcam), or cleaved caspase-3 (1:250 dilution, Cell Signaling Technologies). After washing, sections were incubated with secondary Alexa 594 goat anti-rabbit IgG, Alexa 488-conjugated phalloidin, and Hoechst 33342 (Key Resources Table). In some tissues, mouse anti-E-cadherin was included with the primary antibodies and Alexa 488 goat anti-mouse IgG was included with the secondary antibodies in place of Alexa 488-conjugated phalloidin. Images of tissue sections were collected as stacks at 0.2 μm intervals using an Axioplan 2 (Zeiss), Chroma single channel ET filter sets, 63X NA 1.4 Plan-Apochromat oil immersion objective, and Coolsnap HQ camera. Images were deconvoluted using Autoquant X3 (MediaCybernetics). Images of organoids were collected using a DMI6000 (Leica) with a 63X NA1.3 Plan-Apo glycerol immersion objective, CSUX Yokogawa spinning disc (Andor), Borealis illumination system (Andor), and Zyla Plus camera (Andor). Both microscopes were controlled by MetaMorph 7.8 (Molecular Devices). Images of H&E-stained sections were acquired using a DMLB microscope (Leica) with a 40X NA 0.65 FL-Plan objective, and Micropublisher 3 camera (QImaging) controlled by QCapPro 7 (QImaging).

Histopathological Scoring

Histopathological analysis of colitis was performed by a pathologist blinded to the experimental conditions. Colon tissues were scored on a scale of 0-3 for eight parameters, yielding a maximum score of 24. Scoring parameters were goblet cell depletion, mucosal hyperplasia, crypt cell apoptosis, erosion, lymphocytic infiltrate, polymorphonuclear (PMN) leukocyte infiltrate, crypt architectural distortion, and involvement of the submucosa.

Quantification and Statistical Analysis

All data are representative of at least 3 independent experiments with 3-10 mice per group. Specific numbers of mice per group is annotated in corresponding figure legends. Data are presented as mean ± SEM. Statistical significance was determined by two-tailed Student's t test, two-tailed Mann-Whitney U test, or Kaplan-Meier log-rank test. p values are indicated in the figures (*$p < 0.05$, ** $p < 0.01$, *** $p < 0.001$).